JACS
JOURNAL OF THE AMERICAN CHEMICAL SOCIETY

Article

pubs.acs.org/JACS

Investigation of the Electronic Ground States for a Reduced Pyridine(diimine) Uranium Series: Evidence for a Ligand Tetraanion Stabilized by a Uranium Dimer

Nickolas H. Anderson,[†] Samuel O. Odoh,[‡] Ursula J. Williams,[§] Andrew J. Lewis,[§] Gregory L. Wagner,[∥] Juan Lezama Pacheco,[⊥] Stosh A. Kozimor,[∥] Laura Gagliardi,[‡] Eric J. Schelter,[§] and Suzanne C. Bart*[,†]

[†]H.C. Brown Laboratory, Department of Chemistry, Purdue University, West Lafayette, Indiana 47907, United States

[‡]Department of Chemistry, Supercomputing Institute, and Chemical Theory Center, University of Minnesota, Minneapolis, Minnesota 55455, United States

[§]P. Roy and Diana T. Vagelos Laboratories, Department of Chemistry, University of Pennsylvania, Philadelphia, Pennsylvania 19104, United States

[∥]Los Alamos National Laboratory, Los Alamos, New Mexico 87545, United States

[⊥]School of Earth Sciences, Environmental Earth System Science Department, Stanford University, Stanford, California 94305-4216, United States

Supporting Information

ABSTRACT: The electronic structures of a series of highly reduced uranium complexes bearing the redox-active pyridine(diimine) ligand, $^{Mes}PDI^{Me}$ ($^{Mes}PDI^{Me}$ = 2,6-(2,4,6-Me_3-C_6H_2-N=CMe)$_2C_5H_3N$) have been investigated. The complexes, ($^{Mes}PDI^{Me}$)UI_3(THF) (**1**), ($^{Mes}PDI^{Me}$)UI_2(THF)$_2$ (**2**), [($^{Mes}PDI^{Me}$)UI]$_2$ (**3**), and [($^{Mes}PDI^{Me}$)U(THF)]$_2$ (**4**), were examined using electronic and X-ray absorption spectroscopies, magnetometry, and computational analyses. Taken together, these studies suggest that all members of the series contain uranium(IV) centers with $5f^2$ configurations and reduced ligand frameworks, specifically [$^{Mes}PDI^{Me}$]$^{\bullet/-}$, [$^{Mes}PDI^{Me}$]$^{2-}$, [$^{Mes}PDI^{Me}$]$^{3-}$ and [$^{Mes}PDI^{Me}$]$^{4-}$, respectively. In the cases of **2**, **3**, and **4** no unpaired spin density was found on the ligands, indicating a singlet diradical ligand in monomeric **2** and ligand electron spin-pairing through dimerization in **3** and **4**. Interaction energies, representing enthalpies of dimerization, of −116.0 and −144.4 kcal mol^{-1} were calculated using DFT for the monomers of **3** and **4**, respectively, showing there is a large stabilization gained by dimerization through uranium−arene bonds. Highlighted in these studies is compound **4**, bearing a previously unobserved pyridine(diimine) tetraanion, that was uniquely stabilized by backbonding between uranium cations and the η^5-pyridyl ring.

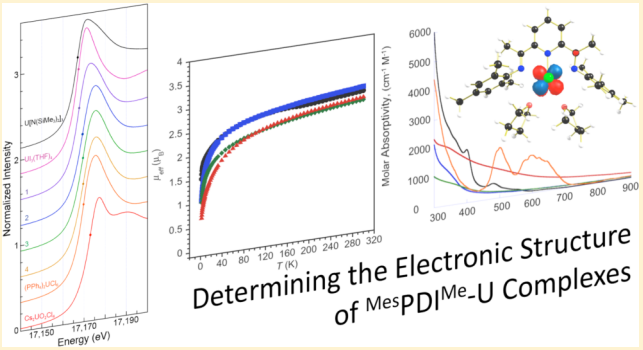

INTRODUCTION

Redox non-innocent ligands have proven to be useful tools in organometallic and inorganic chemistry, due to their mediation of multi-electron processes for metal complexes where such processes could not otherwise occur.[1−7] Ligand-based redox events can sometimes result in "ambiguous" oxidation states at metal centers, as initially articulated by Jørgensen.[8] Thus, ligand non-innocence can lead to unusual bonding and electronic structures, in which traditional electronic descriptions fail to accurately describe the metal−ligand interaction. The development of advanced spectroscopic techniques and computational methodologies has improved our ability to characterize complicated interactions between non-innocent ligands and metals. Often times, no single technique can definitively determine electronic structures of complexes containing ligands that engage in redox chemistry, but combining multiple techniques provides a compelling body of evidence for electronic configuration assignments in these systems. When such data support redox events occurring at both the metal and ligand, the term "redox-active" is most appropriate to describe the ligands.[4]

One such ligand class that has gained popularity in recent years is the 2,6-pyridine(diimine) ligand, $^{R}PDI^{R'}$ ($^{R}PDI^{R'}$ = 2,6-(R-N=CR′)$_2C_5H_3N$), in part due to its utility in the generation of highly active iron and cobalt catalysts for olefin polymerization.[9,10] Since this important discovery, the pyridine(diimine) family has supported a variety of metals that mediate organometallic processes, including but not limited to olefin hydrogenation[11] (asymmetric[12,13]), ester hydrogenation,[14]

Received: November 19, 2014
Published: April 1, 2015

DOI: 10.1021/ja511867a
J. Am. Chem. Soc. 2015, 137, 4690−4700

Scheme 1. Synthesis of Compounds 1−4[a]

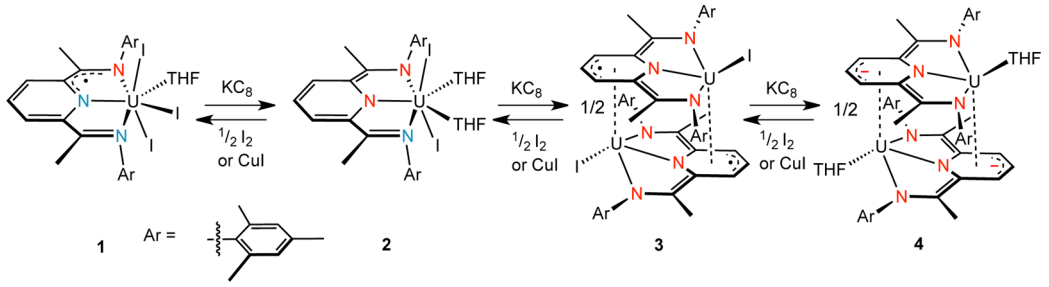

[a]Red N atoms indicate anionic interactions; blue N atoms signify neutral (dative) interactions.

Table 1. Uranium−Nitrogen Distance Comparison for 2−4

bond	**2** (Å)	**3** (Å)	**4** (Å)	(^{Mes}PDI^{Me})UI$_2$(NMes)(THF)
U−N$_{imine}$	2.493(7)	2.410(9)	2.427(7)	2.642(9)
U−N$_{pyridine}$	2.324(9)	2.300(11)	2.305(6)	2.577(7)
U−N$_{imine}$	2.493(7)	2.392(9)	2.407(6)	2.615(8)

olefin and ketone hydrosilylation,[15−18] olefin hydroboration,[19,20] cyclizations,[21−23] reductive cyclizations,[23] lactide polymerization,[24] aldol reactions,[25] and formic acid dehydrogenation.[26] Complementing some of these synthetic studies are investigations of redox chemistry of the pyridine(diimine) metal complexes, which aim to determine their electronic structures and the role ligand non-innocence plays in the observed chemistry.[22,28−44] Combining spectroscopic, crystallographic, and computational techniques have shown that in many cases, especially for first-row transition metals, rather than a low-valent metal center supported by a neutral pyridine(diimine) ligand, a more appropriate description is of an oxidized metal center supported by a reduced chelate. Further, the electrons stored in the ligand framework are highly delocalized throughout the pyridine(diimine) plane.

The utility of pyridine(diimine) ligands in stabilizing transition-metal species prompted an investigation to determine if the pyridine(diimine) framework could act similarly as a vehicle to support electron-rich uranium species. Our initial work demonstrated the feasibility of this postulate with the synthesis of the cyclopentadienyl uranium ^{Mes}PDI^{Me} series (^{Mes}PDI^{Me} = 2,6-(2,4,6-Me$_3$-C$_6$H$_2$-N═CMe)$_2$C$_5$H$_3$N), Cp*UI$_2$(^{Mes}PDI^{Me}), Cp*UI(^{Mes}PDI^{Me}), and Cp*U(^{Mes}PDI^{Me})(THF) (Cp* = η^5-C$_5$Me$_5$), whose members feature uranium(IV) centers ligated by reduced ligands [^{Mes}PDI^{Me}]$^{\bullet/-}$, [^{Mes}PDI^{Me}]$^{2-}$, [^{Mes}PDI^{Me}]$^{3-}$, respectively.[27] The extent of ligand reduction was confirmed by examining ligand metrical parameters as determined by X-ray crystallography. The redox activity of Cp*U(^{Mes}PDI^{Me})(THF) was demonstrated in the cleavage of the strong N═N double bond in azobenzene with three reducing ligand equivalents and one from the uranium cation.[28] With this result in mind, we generated an analogous series of reduced compounds without the cyclopentadienyl substituent.[29] The first compound in the series, (^{Mes}PDI^{Me})UI$_3$(THF) (**1**), was synthesized by addition of neutral ^{Mes}PDI^{Me} to UI$_3$(THF)$_4$. Upon coordination of the ^{Mes}PDI^{Me} ligand, an electron transfer from uranium(III) to ^{Mes}PDI^{Me} ensued, generating a uranium(IV) cation ligated by a radical anion, [^{Mes}PDI^{Me}]$^{\bullet/-}$ and three iodide ligands. In the case of **1**, reliable structural parameters could not be established by X-ray crystallography due to poor crystal quality. The ground-state electronic configuration was established by variable-temperature magnetometry measurements, in which the low-temperature data supported the presence of a ligand radical. The rest of the compounds in the series, (^{Mes}PDI^{Me})UI$_2$(THF)$_2$ (**2**), [(^{Mes}PDI^{Me})UI]$_2$ (**3**), and [(^{Mes}PDI^{Me})U(THF)]$_2$ (**4**), were synthesized by subsequent single electron reductions of complex **1** using KC$_8$ (Scheme 1). High-quality X-ray diffraction data for **2**−**4** highlighted distortions in the intraligand bonds, as compared to the free ^{Mes}PDI^{Me} ligand, consistent with each reduction being ligand-centered rather than metal-centered.[30]

Insight into the electronic structures of **2**−**4** was gained by examining the U−N bond distances for the pyridine(diimine) chelate, which are typically indicators of ligand reduction.[27,31] Data for **2**−**4** are compiled in Table 1 along with a comparison to (^{Mes}PDI^{Me})UI$_2$(NMes)(THF), a uranium(IV) imido species with a neutral ^{Mes}PDI^{Me} ligand. As previously established by our group,[27,28,31] U−N$_{PDI}$ bonds in the range of 2.3−2.4 Å indicate anionic character, arising from the localization of reducing equivalents in the ligand framework, whereas U−N$_{PDI}$ bonds that are 2.5 Å or higher are consistent with dative interactions to a neutral ^{Mes}PDI^{Me} ligand. The U−N$_{PDI}$ distances for **2** indicate two-electron ligand reduction, as they are consistent with those for Cp*UI(^{Mes}PDI^{Me}) and Cp^{P}UI(^{Mes}PDI^{Me}) (Cp^{P} = η^5-C$_5$H$_4$CMe$_2$Ph), both of which were reported to contain [^{Mes}PDI^{Me}]$^{2-}$ ligands.[27] The U−N$_{PDI}$ distances in **3**, along with intraligand parameters, are consistent with those reported for the triply reduced chelate in Cp*U(^{Mes}PDI^{Me})(THF).[28] Thus, based on the short U−N$_{PDI}$ distances contrasting those in (^{Mes}PDI^{Me})UI$_2$(NMes)(THF), **2** and **3** were best described by crystallography as containing uranium(IV) centers supported by [^{Mes}PDI^{Me}]$^{2-}$ and [^{Mes}PDI^{Me}]$^{3-}$ ligands, respectively.

Although compound **4** was formed by reduction of **3**, the ligand oxidation state was more difficult to establish based on structural parameters of **4** alone, since they are statistically indistinguishable from those reported for **3**. The structural analyses of **3** and **4** are complicated by their dimeric nature, which creates steric hindrance between the ^{Mes}PDI^{Me} ligands. Thus, dimerization may be responsible for distortions observed in the bond distances. Dimerization in **3** and **4** results from the uranium centers interacting in an η^5-fashion with the pyridine ring of the opposite ^{Mes}PDI^{Me} ligand, with respective U−C bond distance ranges of 2.725(12)−2.820(11) and 2.707(8)−

DOI: 10.1021/ja511867a
J. Am. Chem. Soc. 2015, 137, 4690−4700

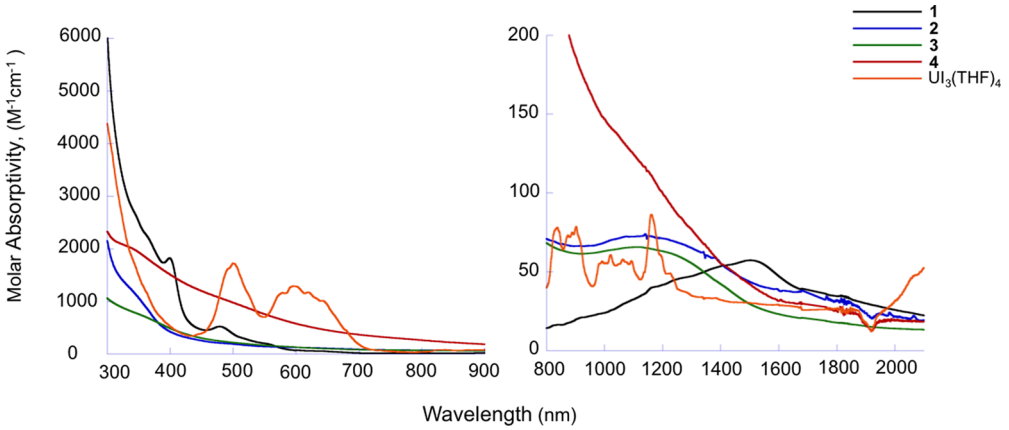

Figure 1. Electronic absorption spectra for compounds **1** (black), **2** (blue), **3** (green), **4** (red), and $UI_3(THF)_4$ (orange, for reference) recorded in THF at ambient temperature. The UV−vis region (left) is from 280 to 900 nm, and the near-infrared region (right) is shown from 800 to 2200 nm.

2.801(8) Å. These η^5 interactions involve the same orbitals as the η^6−arene−uranium interactions, which are well precedented in the actinide literature with the majority of coordinated arenes existing in their reduced form.[50−53] The role of the arene interaction is significant in the formation of dimers **3** and **4**, as highly reduced transition-metal species with pyridine(diimine) ligands have been established to form the bis(ligand) derivatives, $(^{R}PDI^{R'})_2M$, saturating the metal center and preventing further reactivity.[32] With the metal−arene interactions operative, the electronic structure of **4** could be described in several ways when considering charge balance. Compound **4** might result from reduction of the uranium center in **3** to provide a uranium(III) center coordinated by a $[^{Mes}PDI^{Me}]^{3-}$ ligand; alternatively, reduction of the ligand is also possible to generate a uranium(IV) center ligated by $[^{Mes}PDI^{Me}]^{4-}$. Given the highly reducing nature of uranium(III)[33−35] and that a pyridine(diimine) tetraanion has not been previously observed, one can also imagine configurations between these canonical oxidation state assignments.

Despite their complicated electronic structures, compounds **2**−**4** show rich redox chemistry that is easily characterized. For instance, oxidation of **2**, **3**, and **4** with varying equivalents of mesitylazide (N_3Mes) resulted in formation of the corresponding pyridine(diimine) uranium mono-, bis-, and tris(imido) compounds, respectively.[29] Each oxidized species was supported by a neutral $[^{Mes}PDI^{Me}]^0$ ligand, as determined crystallographically, indicating that reducing equivalents stored in the ligand, along with electrons from uranium for **3** and **4**, were used in the activation of the organoazide. Given the formation of the interesting uranium imido products, including the previously unobserved tris(imido) derivative, along with the unprecedented multi-electron redox chemistry, further investigation of **1**−**4** to evaluate their ground-state electronic structures is warranted. Herein, we report the characterization for this unusual family, **1**−**4**, by magnetometry, computational, and electronic, and X-ray absorption spectroscopic measurements supported by redox chemistry.

RESULTS AND DISCUSSION

Electronic Absorption Spectroscopy. Studies on **1**−**4** were initiated using solution-phase electronic absorption spectroscopy, as this technique has been established as a useful tool in elucidating the oxidation states of redox-active ligands[45,57] and low- and mid-valent uranium species.[58−60] This technique can be helpful in differentiating uranium centers of varying oxidation states, as near-infrared and UV−vis spectra provide fingerprints for compounds with uranium $5f^0$, $5f^1$, $5f^2$, and $5f^3$ configurations. Data for complexes **1**−**4** were collected from 280−2200 nm at ambient temperature in THF and are presented in Figure 1, along with the spectrum of $UI_3(THF)_4$ for comparison.

From previous studies,[29] compound **1** was found to include a radical delocalized throughout the plane of the $[^{Mes}PDI^{Me}]^{\bullet/-}$ ligand, thus its absorption spectrum should be unique as compared to **2**−**4**. Inspection of the UV and visible regions for **1** indeed show a more pronounced absorption profile as compared to complexes **2**−**4**. For compound **1**, the absorption at 399 nm (1824 M^{-1} cm^{-1}) is similar to that observed for the family of tetravalent uranium complexes $(NN^R)UI_2(THF)$ (NN^R = fc(NR)$_2$, fc =1,1′-ferrocenediyl, R = $SiMe_3$, Si^tBuMe_2, $SiMe_2Ph$), which have similar absorptions in the 400−500 range with modest molar absorptivities (1100−1900 M^{-1} cm^{-1}) and are indicative of 5f−6d transitions within the uranium ion and iodide-uranium charge-transfer transitions.[36] This is also reminiscent of [((^{t}BuArO)$_3$tacn)U(dbabh)], which has an absorption at 408 nm (1943 M^{-1} cm^{-1}).[37] Compound **1** displays a second absorption at 479 nm (522 M^{-1} cm^{-1}), similar to the uranium-iodide charge transfer observed previously in tetravalent $UI_4(OEt_2)_2$ as well,[36] albeit with a lower molar absorptivity. Comparing the absorption profiles throughout the visible region in the spectra of **1** with $UI_3(THF)_4$ shows spectral characteristics, with significantly higher molar absorptivities in the trivalent case,[38] supporting the uranium(IV) oxidation state in **1**. While the UV and visible regions for **2**−**4** are similar to each other, they are strikingly different when compared to **1**. The well-defined bands seen for **1** are absent and are replaced by broadened transitions. These absorptions have line shapes and molar absorptivities that are comparable to those observed for the uranium(IV) ion in $(NN^R)U(CH_2Ph)_2(THF)$.[36] As with this family of heterobimetallic species, **2**−**4** have strong absorptions at ∼300 nm (1500−4000 M^{-1} cm^{-1}), which may indicate 5f−6d transitions within the uranium core. These line shapes are similar to those in the tetravalent ketimido derivative $Cp^*_2U[N{=}C(Ph)_2]_2$ (∼10,000 M^{-1} cm^{-1}) but have significantly lower molar absorptivities.[39]

Examination of the near-infrared spectra for **1**−**4** further highlights the differences in these complexes. The spectrum for **1** shows a broad band spanning 1200−1800 nm, which is

DOI: 10.1021/ja511867a
J. Am. Chem. Soc. 2015, 137, 4690−4700

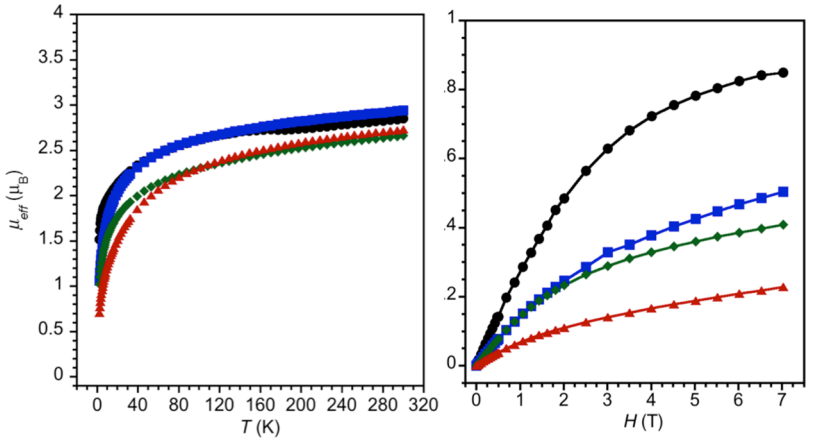

Figure 2. Variable-temperature molar magnetic data (μ_{eff}) for **1** (black, ●),[29] **2** (blue, ■), **3** (green, ◆), and **4** (red, ▲) (left) and variable field data collected at 2 K (right). Data plotted per uranium ion. Lines are provided as guides to the eye.

Table 2. Summary of Magnetic Data for Compounds 1−4 and Selected Literature Benchmarks

compound	uranium oxidation state	$^{Mes}PDI^{Me}$ oxidation state	μ_{eff} (300 K, μ_B)	μ_{eff} (2/5 K, μ_B)	M (2 K, 7 T, μ_B)
$[((^{Ad}ArO)_3tacn)U]$	III	−	2.75[a]	1.73	[b]
$[((^{Ad}ArO)_3tacn)U(CO_2^{\bullet -})]$	IV	−	2.89	1.51	[b]
$[((^{Ad}ArO)_3tacn)U(N_3)]$	IV	−	2.85[a]	0.70[a]	[b]
1	IV	−1	2.85	1.52	0.85
2	IV	−2	2.94	1.06	0.50
3	IV	−3	2.66	1.03	0.41
4	IV	−4	2.73	0.71	0.23

[a]Estimated from graphical data reported in ref 43. [b]Not reported.

shifted as compared to the similar broad bands observed for **2**−**4**. The molar absorptivities of these transitions (50−100 M^{-1} cm^{-1}) are in line with those observed for previously published uranium(IV) complexes containing redox-innocent ligands,[38−40] however, the bands in **1**−**4** are broader than those typically observed. Previous studies have shown that f−f transitions are difficult to resolve in the presence of uranium−amine and uranium−arene functionalities, owing to intense charge transfer bands as has been noted in $[((^tBuArO)_3Mes)U]$. Further, the broadness observed for **1** contrasts those for other tetravalent uranium species with radical anionic ligands. $[((^{t\text{-}Bu}ArO)_3tacn)U(\eta^2\text{-}NNCPh_2^{\bullet})]$,[41] $[((^{t\text{-}Bu}ArO)_3tacn)U(OC^{t\text{-}Bu}Ph_2^{\bullet})]$,[42] and $[((^{Ad}ArO)_3tacn)U(CO_2^{\bullet})]$[43] all display sharp but weak f−f transitions characteristic of the uranium(IV) oxidation state, but in these cases, the radical electron is localized on the axial ligand in the seventh coordination site, rather than delocalized. While the electronic absorption spectra do support the initial assignments of the uranium series **1**−**4** as containing tetravalent uranium centers, these data do not provide definitive assignments of electronic configurations on their own. Additional analytical tools were enlisted to more thoroughly probe the electronic structure of these species.

Magnetometry Studies. Variable-temperature and field-dependent magnetic measurements were performed to further elucidate the electronic structures and spin states of paramagnetic complexes **1**−**4**, with an emphasis on establishing the ligand and uranium oxidation state in **4**. In general, room-temperature magnetic data alone do not allow differentiation between U(III) and U(IV) complexes due to their similar expected Curie magnetic moments.[44] Using L−S coupling, the predicted RT moment for the $^3H_4$ U(IV) ion is 3.58 μ_B, while that for the $^4I_{9/2}$ U(III) ion is 3.62 μ_B. In both cases, the observed moments are typically smaller than the predicted ones, due to ligand field states that split the J = 4 or 9/2 ground terms by more than kT at room temperature.[45−48] Data for **2**−**4** are plotted with data previously reported for **1**[29] for comparison in Figure 2. For compound **1**, the variable-temperature μ_{eff} data showed a depopulation of ligand field states consistent with a $5f^2$ $^3H_4$ uranium(IV) cation. At low temperatures, the magnetic behavior of **1** was dominated by $[^{Mes}PDI^{Me}]^{\bullet/-}$ ligand radical. This is further supported by the magnetization versus field curve for **1** at 2 K, which showed the onset of magnetic saturation with a value of 0.85 μ_B at 7.0 T, close to the theoretical value of 1.00 μ_B for a $[^{Mes}PDI^{Me}]^{\bullet/-}$ ligand radical when g = 2.0. Thus, the magnetometry data for **1** supported an electronic structure assignment of a $5f^2$ uranium(IV) ion and a radical $^{Mes}PDI^{Me}$ ligand (doublet). Ligand radical character was supported by EPR spectroscopy, which shows a room-temperature signal at g = 2.0016 (Figure S13).

The magnetic data for complexes **2**−**4**, provided on a per ion basis, are very similar to each other and to complex **1** (Figure 2 and Table 2). The temperature dependences of **2**−**4** similarly follow a monotonic decrease with temperature as with **1**, also indicating depopulation of ligand field levels due to the uranium cations. All the compounds **1**−**4** show μ_{eff} values at 300 K in a small range of 2.66−2.94 μ_B, characteristic of uranium(IV) cations.[45,49−51] The μ_{eff} values at 2 K for **2**−**4** also fall in a small range of low values from 0.71−1.06 μ_B per uranium cation. Unlike complex **1**, complexes **2**−**4** exhibit a gradual increase in their magnetization versus field data at 2.0 K and do not approach magnetic saturation. The range of values obtained for **2**−**4** at 7.0 T is 0.23−0.50 μ_B. The similarities in

DOI: 10.1021/ja511867a
J. Am. Chem. Soc. 2015, 137, 4690−4700

the field- and temperature-dependent data for **2**−**4** are surprising, given the range and extent of their reduction. The room-temperature moments, temperature dependences, and low-temperature field-dependent data taken together suggest that all members of the series include uranium(IV) cations.

The range of high-temperature moments for **1**−**4** is similar to those observed by Meyer and co-workers for $[((^{Ad}ArO)_3tacn)U^{III}]$ and $[((^{Ad}ArO)_3tacn)U^{IV}(L)]$ (L = $CO_2^{\bullet/-}$ or N_3^-; $((^{Ad}ArOH)_3tacn$ = 1,4,7-tris(3-adamantyl-5-*tert*-butyl-2-hydroxybenzyl)1,4,7-triazacyclononane) (Table 2).[43] In the Meyer series, the oxidation states of U(III) and U(IV) were assigned on the basis of $[((^{Ad}ArO)_3tacn)U^{III}]$ having a ligand field doublet ground state from its $5f^3$ configuration that retained a moment of 1.5 μ_B at 2 K, whereas the $5f^2$ $[((^{Ad}ArO)_3tacn)U^{IV}(N_3)]$ exhibited a ligand field singlet with only a small moment ∼0.5 μ_B at 2 K. Similar to complex **1**, $[((^{Ad}ArO)_3tacn)U^{IV}(CO_2)]$ exhibited a LT moment of ∼1.51 μ_B, attributed to the single unpaired electron on the $CO_2^{\bullet/-}$ ligand and a non-magnetic singlet from a uranium(IV) ion.

Given the similar temperature- and field-dependent magnetic data for **2**−**4** and the data reported by Meyer, the data support the postulate that compounds **2**−**4** all contain uranium(IV), $5f^2$ centers. Furthermore, the low-temperature data points to the absence of unpaired spins on the $^{Mes}PDI^{Me}$ ligand frameworks for **2**−**4**. Using charge balance, complex **2** contains two iodide ligands and a dianionic $[^{Mes}PDI^{Me}]^{2-}$ ligand, whereas complex **3** contains one iodide ligand with a $[^{Mes}PDI^{Me}]^{3-}$ moiety. Similarly in complex **4**, each uranium(IV) cation is coordinated by a formally $[^{Mes}PDI^{Me}]^{4-}$ ligand such that the paramagnetism is only due to the $5f^2$ configuration. These magnetic data corroborate the findings from the electronic absorption measurements. The dimeric nature of complexes **3** and **4** facilitates spin pairing of the six $[^{Mes}PDI^{Me}]_2^{6-}$ or eight $[^{Mes}PDI^{Me}]_2^{8-}$ ligand electrons per dimer as supported by DFT calculations (*vide infra*). Overall, the magnetic data for **1**−**4** indicate the reducing equivalents in this system for the activation of small molecules reside primarily in the ligands.

X-ray Absorption Near Edge Spectroscopy. To further probe the valency at the uranium center, X-ray absorption near edge spectroscopy (XANES) was used. Data were collected in transmission mode at the Stanford Synchrotron Radiation Lightsource (SSRL) on beam line 11-2 (See Supporting Information for experimental details). The background subtracted and normalized U L_{III}-edge XANES spectra for **1**−**4** are presented in Figure 3. Collectively, the spectra are similar to other U L_{III}-edge XANES reports of formally tri- and tetravalent uranium compounds, in that they contain a single edge peak between 17167 and 17170 eV superimposed on a step-like absorption threshold.[52−57] From the perspective of the free ion, the edge features in these spectra primarily originate from electric-dipole allowed transitions from uranium 2p orbitals to unoccupied states that contain U d- and s-character, e.g., for tetravalent uranium a $2p^6\cdots5f^26d^0 \rightarrow 2p^5\cdots5f^26d^1$ transition is expected. The step-like absorption threshold represents the ionization potential of the uranium ion. It has been shown that the energy of the first inflection point of the rising X-ray absorption edge could be correlated with the effective nuclear charge of the absorbing uranium atom.[52−57] However, it has been well documented that many factors influence the exact absorption energy, i.e., the coordination geometry and amount of orbital mixing in a given uranium−

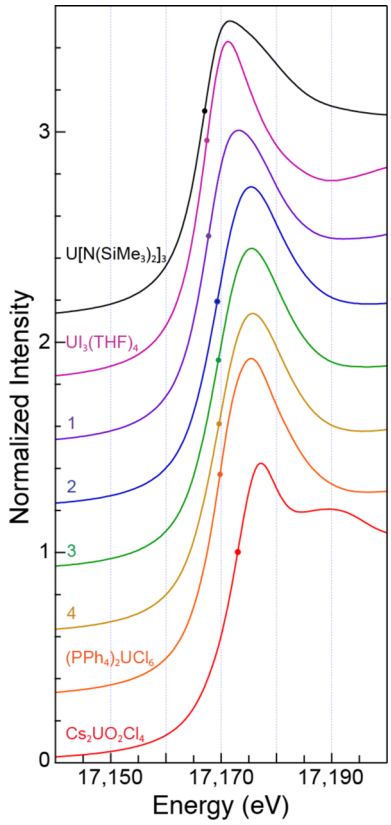

Figure 3. U L_{III}-edge XANES from the following compounds listed top to bottom; $U[N(SiMe_3)_2]_3$ (black trace), UI_3THF_4 (indigo trace), **1** (violet trace), **2** (blue trace), **3** (green trace), **4** (yellow trace), $(PPh_4)_2U^{IV}Cl_6$ (orange trace), and $Cs_2U^{VI}O_2Cl_4$ (red trace). The circular markers represent the inflection point.

ligand bond. Herein, we have compared the inflection point energies for compounds **1**−**4** with that of tri- and tetravalent uranium standards, namely $U^{III}[N(SiMe_3)_2]_3$,[58−60] $U^{III}I_3(THF)_4$,[61,62] and $(PPh_4)_2U^{IV}Cl_6$.[63] These inflection points were quantified by determining the point at which the second derivative of the data equals zero, and the results are represented graphically as the circular markers in Figure 3 and summarized in Table 3.

The data for **1**−**4** and the standards were calibrated to the yttrium K-edge from a yttrium calibration foil (17038.4 eV) measured *in situ*. However, to better compare our experimental values with those previously published on some tri- and tetravalent uranium complexes, the energy difference between the inflection points determined for hexavalent $Cs_2UO_2Cl_4$[64] and compounds **1**−**4**, $U^{III}[N(SiMe_3)_2]_3$, $U^{III}I_3(THF)_4$, and $(PPh_4)_2U^{IV}Cl_6$ were also calculated and tabulated in Table 3. The −6.2 eV energy difference between $U^{III}[N(SiMe_3)_2]_3$ and $Cs_2UO_2Cl_4$ measured here is in excellent agreement with the −6.3 eV value reported by Lukens and co-workers.[52] Similarly, the energy for the $U^{III}I_3(THF)_4$ inflection point was −5.8 eV lower than that of $Cs_2UO_2Cl_4$. The rising edge for the $(PPh_4)_2U^{IV}Cl_6$ standard was approximately 2 eV higher in energy than the trivalent standards and found to be −3.4 eV from $Cs_2UO_2Cl_4$. Although the inflection points for compounds **1**−**4** were bracketed by the tri- and tetravalent standards, the energy value for compound **1** (−5.4 eV from $Cs_2UO_2Cl_4$) was approximately 2 eV lower than that of **2**−**4**, which was on average −3.7 eV from $Cs_2UO_2Cl_4$.

DOI: 10.1021/ja511867a
J. Am. Chem. Soc. 2015, 137, 4690−4700

Table 3. Energy for the First Inflection Point of the U L_{III}-Edge XANES Data from Compounds 1−4 vs Formally Tri- and Tetravalent Standards[a]

compound	inflection point (eV)	inflection point minus that of $Cs_2UO_2Cl_4$ (eV)
$U[N(SiMe_3)_2]_3$	17,167.0	−6.2
$UI_3(THF)_4$	17,167.4	−5.8
1	17,167.7	−5.5
2	17,169.3	−3.9
3	17,169.5	−3.7
4	17,169.6	−3.6
$U(^{Mes}DAB^{Me})_2(THF)$[5]	17,169.32[b]	−3.9
$U(C_5H_5)_2(^{Mes}DAB^{Me})$[5]	17,169.32[b]	−3.9
$(PPh_4)_2UCl_6$	17,169.8	−3.4
$Cs_2UO_2Cl_4$	17,173.2	0.0

[a]Also included are the differences in inflection point energies from that of $Cs_2UO_2Cl_4$. All data are calibrated against the Y K-edge from an Y foil measured *in situ* (17038.04 eV). [b]In the original report[56] the U L_{III}-edge spectra were calibrated to the yttrium K-edge of our yttrium calibration foil at 17032.08 eV. Values for $U(^{Mes}DAB^{Me})_2(THF)$ and $Cp_2U(^{Mes}DAB^{Me})$ have been reworked using the latest calibration value of 17038.4 eV.

Using the inflection point metrics described above, compounds **2**−**4** exhibited spectra similar to that of $(PPh_4)_2U^{IV}Cl_6$. Consequently, these values also agreed quite well with our recent U L_{III}-edge XANES analyses for $U(^{Mes}DAB^{Me})_2(THF)$ and $Cp_2U(^{Mes}DAB^{Me})_2$.[56] To facilitate comparison with compounds **1**−**4**, data in the original report were recalibrated to 17038.4 eV, and the results showed inflection points that were offset by −3.9 eV from that of $Cs_2UO_2Cl_4$. Hence, the U L_{III}-edge XANES suggested that descriptions of **2**−**4** invoking $5f^2$ uranium ions and $[^{Mes}PDI^{Me}]^{2-}$, $[^{Mes}PDI^{Me}]^{3-}$, and $[^{Mes}PDI^{Me}]^{4-}$ ligands, respectively, were appropriate. Surprisingly, the data for compound **1** closely resembled that of $U^{III}[N(SiMe_3)_2]_3$ and $U^{III}I_3(THF)_4$. Based on these data alone, it is tempting to describe **1** (under these experimental conditions) as having a neutral $^{Mes}PDI^{Me}$ ligand and a uranium atom with three relatively localized 5f electrons. However, the inflection point for **1**, which contains three nitrogen donors and three iodide donors, was still 0.7 eV higher than that of the trisamido $U[N(SiMe_3)_2]_3$ complex and 0.3 eV higher than triiodide $UI_3(THF)_4$ complex. Given the electronic absorption spectroscopic measurements and the magnetometry data (described earlier) as well as the DFT calculations (*vida infra*), we attribute the difference in rising edge positions to substantial orbital mixing between a $[^{Mes}PDI^{Me}]^{\bullet/-}$ radical anion, the iodine ligands, and the uranium metal center. Hence, in spite of the limitations associated with formal oxidation state assignments, we believe that the most reasonability description of compound **1** is as containing a U(IV) ion with covalent U−$^{Mes}PDI^{Me}$ and/or U−I bonding interactions. Future work is focused on attempting to better characterize the U−N($^{Mes}PDI^{Me}$) interaction using N K-edge X-ray absorption spectroscopy.

Computational Analysis. *Monomeric Species, 1 and 2.* To further probe the metal and ligand oxidation states in **1** and **2**, geometry optimizations were performed, and their calculated structural parameters from the PBE functional are tabulated (Table 4, Figure 4). Because reliable metrics from crystallography could not be determined for compound **1**, its calculated U−N bond distances (2.467 (U−N_{pyr}) and 2.623 Å) do not have the benefit of an experimental comparison to the same molecule. However, these distances can be compared to the U−N distances in $Cp^PUI_2(^{Mes}PDI^{Me})$ (2.522(10), 2.368(10) (U−N_{pyr}), and 2.484(9) Å) and $Cp^PU(O_2C_2Ph_4)(^{Mes}PDI^{Me})$ (2.679(4), 2.434(4) (U−N_{pyr}), and 2.607(4) Å), both of which have been established to have monoanionic $[^{Mes}PDI^{Me}]^{\bullet/-}$ ligands by X-ray crystallography and SQUID magnetometry.[27]

Table 4. Calculated Bond Lengths for 1 and 2 and Experimental Bond Lengths for $Cp^PU(O_2C_2Ph_4)(^{Mes}PDI^{Me})$ and 2. The calculated structural parameters were obtained with the PBE functional. U−I_{ax} and U−I_{eq} are the axial and equatorial U−I bond lengths, respectively

	1	$Cp^PU(O_2C_2Ph_4)(^{Mes}PDI^{Me})$	**2**	
	calcd (Å)	expt. (Å)	calcd (Å)	expt. (Å)
U−N1	2.623	2.607(4)	2.518	2.493
U−N2	2.467	2.434(4)	2.318	2.324
U−I_{ax}	3.013	–	3.068	3.080
U−I_{eq}	3.039	–		
U−O_{THF}	2.492	–	2.604	2.546
N1−C2	1.320	1.305(6)	1.349	1.377
N2−C3	1.319	1.383(7)	1.343	1.369
C2−C3	1.450	1.440(7)	1.416	1.400
C3−C4	1.398	1.384(7)	1.398	1.414
C4−C5	1.392	1.385(8)	1.393	1.373

The Mulliken spin density for the uranium center in **1** was calculated to be ∼2.3; although this value is slightly higher than expected for a pure U(IV) ion, it is still in an acceptable range for the U-$5f^2$ configuration.[65,66] The corresponding spin density for the $^{Mes}PDI^{Me}$ ligand in **1** was calculated to be ∼0.7, suggesting population of an energetically low-lying ligand π^* orbital by a single electron, supporting the formulation of a monoanionic $[^{Mes}PDI^{Me}]^{\bullet/-}$. This description is consistent with the magnetic data for **1**. Inspection of the Kohn−Sham orbitals of **1** shows that the HOMO and HOMO-1 orbitals (Figure 4) contain two singly occupied 5f orbitals with unpaired electron density, consistent with a uranium(IV) center. The additional unpaired electron in **1** is situated in the HOMO-2 orbital, whose parentage is primarily ligand in character (∼80%). However, this HOMO-2 orbital also has a moderate degree of uranium character, ∼18% 5f and 2% 6d, where some unpaired electron density is present. This is likely to explain the elevated spin density value found for the uranium atom, as the π^* of the $^{Mes}PDI^{Me}$ ligand has significant overlap with the uranium 5f orbitals. However, we cannot rule out that the magnitude of this value could be due to the propensity of GGA functionals to delocalize electron density.

As hybrid functionals often favor the localization of electrons, and systems with redox active ligands are generally delocalized, the presence of a ligand radical in compound **1** was also probed using the PBE0 functional, by constraining the unpaired electrons in two different configurations. The first model considered had three unpaired electrons all localized in uranium orbitals giving rise to a neutral ligand, $(^{Mes}PDI^{Me})^0$, and U(III) center, while the second model constrained one electron to $(^{Mes}PDI^{Me})^{\bullet/-}$, leaving two unpaired electrons on uranium, and U(IV). The former configuration, $(^{Mes}PDI^{Me})^0$ and U(III), was confirmed to be an excited state relative to the latter configuration, $(^{Mes}PDI^{Me})^{\bullet/-}$ and U(IV), by using time-dependent DFT with both the PBE and PBE0 functionals. The energy of this ligand-to-metal charge transfer (LMCT) is approximately 11.8 kcal/mol (2431.1 in nm) (see Supporting

DOI: 10.1021/ja511867a
J. Am. Chem. Soc. 2015, 137, 4690−4700

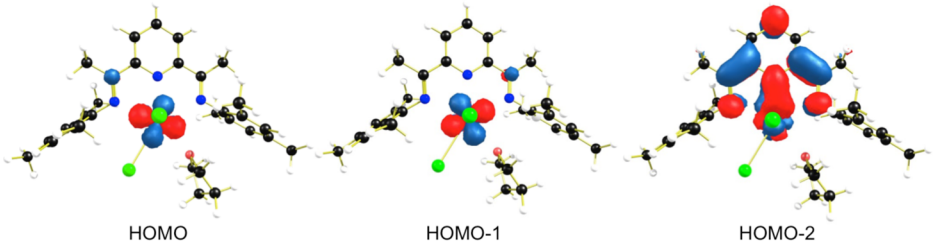

Figure 4. Kohn–Sham orbitals of **1** obtained at the PBE/TZ2P level of theory. These orbitals are of 5f, 5f, and $^{Mes}PDI^{Me}$ in characters, respectively.

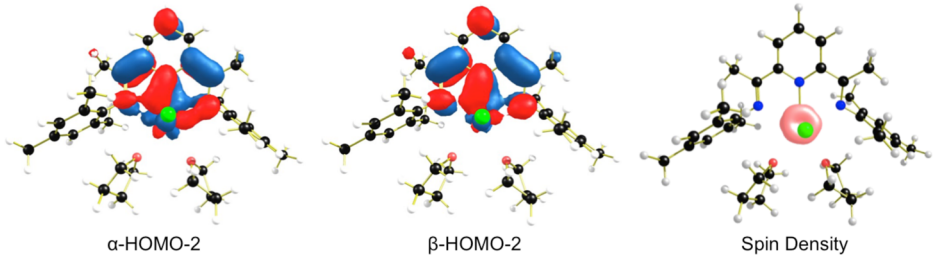

Figure 5. HOMO-2 orbital of **2** containing an electron of both α- and β-spin. These orbitals are primarily ligand in character and have similar eigenvalues. Spin density plot for **2**, showing unpaired spin density is localized on uranium rather than the ligand.

Information). Thus, formation of **1** most likely involves coordination of neutral $^{Mes}PDI^{Me}$ to the uranium(III) center, followed by a metal to ligand charge transfer, which generates a $[^{Mes}PDI^{Me}]^{\bullet/-}U(IV)$ monomer. This analysis supports the assignment that the U $5f^2$ bearing a radical ligand configuration is indeed the lowest energy, electronic ground state of **1**, and is consistent with the electronic absorption spectroscopic and low-temperature magnetic data.

For compound **2**, the calculated structure from the PBE functional is an accurate model for the experimentally determined metrical parameters, as shown by agreement of the calculated bond lengths generally within 0.03 Å of the crystal structure (Table 4). An exception to this is the $U-O_{THF}$ bond distances for **2**, which are overestimated by ~0.06 Å. The calculated Mulliken spin density for the uranium center of ~2.2 compares favorably with that calculated for **1**, supporting that **2** is a uranium(IV) species. By charge balance considerations for neutral **2**, the $^{Mes}PDI^{Me}$ ligand should be reduced by two electrons, which is supported by the parameters observed in the solid-state structure. Confirmation of ligand reduction is seen in the visualization of the valence orbitals of **2**, where the HOMO-2 α-spin orbital is nearly identical to that in **1** (Figure 5). In both cases, this orbital consists primarily of ligand unpaired electron density, with only partial contribution from the uranium center (27.2% 5f and 1.5% 6d). The HOMO β-spin orbital of **2** is analogous to the HOMO-2 α-spin orbital, with both having identical atomic orbital contributions and eigenvalues. Furthermore, the HOMO and HOMO-1 α-spin orbitals of **2** are similar to those in **1** in that they are primarily 5f in nature and thus confirm the assignment of **2** as a U(IV) ion with a ligand dianion, $[^{Mes}PDI^{Me}]^{2-}$ (Figure S3).

Next, the electronic structure of the dianionic $[^{Mes}PDI^{Me}]^{2-}$ ligand was further explored. To determine if the ligand electrons are paired, resulting in a singlet, closed-shell configuration, or unpaired, giving an open shell ligand triplet. Examining the spin density plot for **2** confirms the singlet configuration (Figure 5), which shows that unpaired electron density is localized exclusively on the uranium center, with no ligand participation. The spin density value for the ligand has also dropped to approximately zero (~ −0.1), which is in contrast to **1** (~0.7) and confirms that the electronic structure of $[^{Mes}PDI^{Me}]^{2-}$ is best described as a singlet, corroborating the low-temperature magnetometry data which depicts a singlet ground state. The ligand triplet, corresponding to an overall quintet electronic state for **2**, is about 5.15 kcal/mol higher in energy, suggesting it is not the preferred electronic arrangement. The U–N bonds are significantly shorter in **2** as compared to **1** as a result of the greater electrostatic interactions between the U(IV) center and the $[^{Mes}PDI^{Me}]^{2-}$ as compared to a configuration comprising a U(III) center and $(^{Mes}PDI^{Me})^{\bullet/-}$ ligand. Further confirmation of the ground states of **1** and **2** was obtained by inspection of the Nalewajski–Mrozek[67] bond indices, which include ionic contributions to the interatomic bonds. For the U–N bonds in **1**, these values range between 0.64 and 0.78, while for **2** this range is 0.76 to 1.21, establishing ligand electronic ground states of $[^{Mes}PDI^{Me}]^{\bullet/-}$ and $[^{Mes}PDI^{Me}]^{2-}$ for **1** and **2**, respectively. The calculated U–N distances for **1** are elongated with respect to the experimentally determined structure of **2**, indicating a lesser extent of ligand reduction for **1** as compared to **2**, further supporting assertions for their mono- and dianionic ligand assignments.

Dimeric Species, 3 and 4. Geometry optimizations were performed to understand the electronic structures of dimeric **3** and **4**, but due to their complexity, they were handled separately from monomeric **1** and **2**. Using the PBE functional, the geometry optimization of **3** had good agreement with the experimental values (Tables 5 and S1), with the largest deviation between the calculated and experimental bond lengths being only ~0.04 Å. Single point calculations performed on the experimental and optimized structures of **3** show that the broken-symmetry singlet state is the ground state at the DFT level. The PBE functional shows this singlet ground state for **3** is approximately 4.2, 10.6, 12.1, and 49.9 kcal/mol more stable than the triplet, quintet, septet, and nonet states, respectively. The calculated spin densities for the uranium centers in **3** are between 1.8 and 2.1 (DFT), confirming a $5f^2$ electronic configuration (Table S2), which is supported by

DOI: 10.1021/ja511867a
J. Am. Chem. Soc. 2015, 137, 4690–4700

Table 5. Calculated and Experimental Bond Lengths (Å) in 3 and 4

	3		4	
	calcd	expt.	calcd	expt.
U–N1	2.419	2.392(9)	2.431	2.427(7)
U–N2	2.303	2.300(11)	2.310	2.305(6)
U–I	3.008	3.0157(10)		
U–U	3.703	3.741	3.686	3.668
$U–O_{THF}$			2.603	2.525(6)

examination of the Kohn–Sham orbitals (Figure S4) and magnetic data. By charge balance considerations, a uranium(IV) oxidation state for neutral **3** means the pyridine(diimine) must be reduced by three electrons, which is not surprising given the third reduction of the $^{Mes}PDI^{Me}$ ligand has recently been established for s,[68] d,[69] and f-block[27,28,31] metals. However, the calculated spin densities for the ligands in **3** are negligible, suggesting no radicals are present despite the fact that they are each reduced by three electrons (Figure 6). Thus, the distribution of unpaired spin density and the presence of α- and β-spin orbitals suggest that **3** is formally a $[U^{4+}]_2I_2[(^{Mes}PDI^{Me})_2{}^{6-}]$ system, containing four unpaired electrons populating *only* four uranium 5f orbitals.

As with **2** and **3**, the optimized structure of **4** compares favorably with the experimental results (Table 6). Single-point DFT calculations on the experimental geometry of **4** also reveal a broken-symmetry unrestricted singlet ground state (Tables 6 and S3). Energetically, the quintet state, containing four unpaired electrons, is only slightly higher (~0.5–1.3 kcal/mol) in energy with respect to the singlet ground state and is found whether the local or hybrid functionals are employed. This would imply the quintet state would be partially populated at room temperature; however, there is no evidence for such a population in the magnetometry data. This discrepancy could be due to the fact that DFT can have difficulty handling the broken-symmetry multireference nature of the $S = 0$ state. As such, the energies of the true singlet wave function is likely lower than what is obtained by DFT. For the ground state, the calculated Mulliken spin densities on the uranium atoms in **4** vary from 2.2 to 2.4 (Table 6). Again, these spin densities are elevated for canonical uranium(IV) centers but are on the order of those seen for **2**. Examination of the orbitals of **4** reveals that each uranium center has a $5f^2$ electronic configuration, by the occupation of two orbitals, HOMO and HOMO-1, that are primarily 5f in character (Figure 7).

As evident from the experimental and calculated structures, dimeric **3** and **4** are partially stabilized by the N_2U_2-cores between the pyridine nitrogen atoms of each $^{Mes}PDI^{Me}$ and the opposing uranium centers. The N_2U_2 core is characterized by an outer σ-type ring and an inner accumulation of electron density between the pyridine nitrogen atoms and the two uranium centers (Figure 7, HOMO-4). Further stability for **3** and **4** can be attributed to the interactions between the π^* orbitals of the pyridine in $^{Mes}PDI^{Me}$ and the corresponding 5f orbitals on the opposing uranium centers, which can be characterized as δ-backbonding interactions (Figure 7). This type of bonding mode has been identified previously for reduced toluene and benzene complexes bearing bulky amide[51,53,37] and cyclopentadienyl[50] ligands. In the cases of **3** and **4**, the extreme steric hindrance of the dimeric species prevents a meaningful discussion of bond distances, as the longer U–C distances (2.707(8)–2.820 Å) are out of range as compared to these sterically less encumbered systems.

In the synthesis of **4** from **3**, reductive cleavage of two U–I bonds results in two additional electrons that must be accommodated. These electrons are housed in a fourth ligand π^* orbital, one of α- and one of β-spin that is unoccupied in **3** (Figure 7, HOMO-2). These results suggest that the π^* manifold of the $^{Mes}PDI^{Me}$ ligand is populated by four electrons in **4**, suggesting that the $[^{Mes}PDI^{Me}]^{4-}$ electronic state is indeed accessible in this dimeric coordination geometry through an additional π-backbonding interaction. Thus, compound **4** is assigned as an $[U^{IV}]_2[(^{Mes}PDI^{Me})_2]^{8-}$ electronic system. This broken-symmetry solution is stable with respect to electronic excitation within the time-dependent DFT formalism. Thus, all the reduction processes leading to **2**–**4** appear to be ligand based, and a uranium(IV) center is retained in the compounds at this level of theory.

The interaction energies, or the energies of dimerization, of the monomers of **3** and **4**, were calculated at the PBE/ZORA/STO-TZ2P level. This ΔH value describes the extent of stabilization obtained by dimerization of the monomers (eq 1).

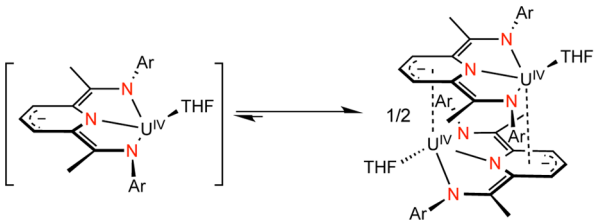

For compound **3**, the energy of dimerization was found to be −116.0 kcal/mol and has a lower absolute value as compared to that for **4**, calculated to be around −144.4 kcal/mol. Thus, **4** is considered to be more stable than **3**, which follows logically

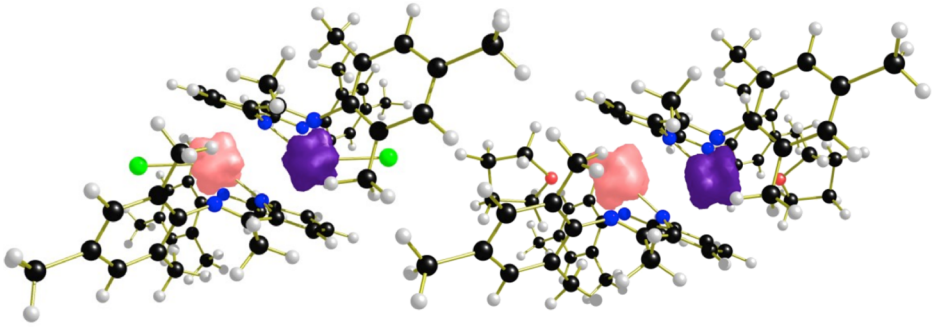

Figure 6. Spin density plots for complexes **3** (left) and **4** (right), showing unpaired electron density is localized on uranium rather than the ligand.

DOI: 10.1021/ja511867a
J. Am. Chem. Soc. 2015, 137, 4690–4700

Table 6. Relative Energies and Mulliken Spin Densities of the Various Electronic States of 4 Obtained with DFT[a]

	broken-symmetry singlet	triplet	quintet	septet	nonet
Relative energies (kcal/mol)					
PBE	0.0	10.6	1.2	12.0	48.3
M06-L	0.0	31.0	0.5	12.1	25.6
PBE0	0.0	54.7	1.5	30.3	38.8
Spin densities					
PBE	2.3(0.0)	1.2(−0.2)	2.4(−0.3)	2.7(0.3)	3.0(0.9)
M06-L	2.4(0.1)	1.2(−0.2)	2.5(−0.4)	2.9(0.2)	3.3(0.7)
PBE0	2.2(0.0)	1.2(−0.1)	2.3(−0.1)	2.6(0.4)	3.0(1.0)

[a]The spin densities on $^{Mes}PDI^{Me}$ are given in parentheses.

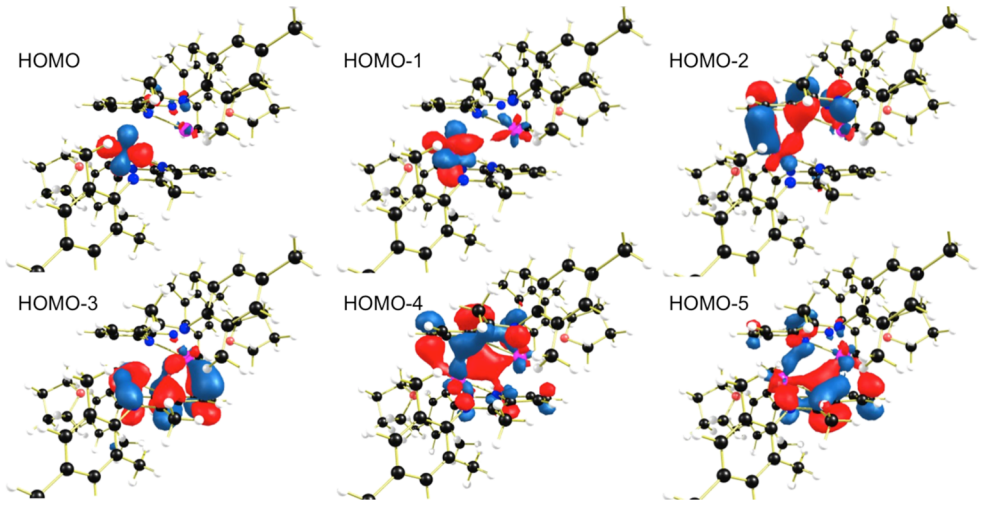

Figure 7. α-spin Kohn−Sham orbitals of the broken-symmetry singlet ground state of 4.

from the presence of the additional δ-backbonding interaction in 4. This is observed experimentally, as 4 is stable in the solid state at room temperature for days, whereas decomposition of 3 is noted after several hours under the same conditions. To further examine the stability of 4, dispersion corrections at the DFT-D3[70] level were included in the computational analysis. Without the dispersion considerations, 4 is calculated to be 28.4 kcal/mol more stable than 3. This value decreases only slightly to approximately 23.3 kcal/mol with the inclusion of the dispersion correction. Thus, 4 is considerably more stable than 3, as inclusion of long-range dispersion effects[71] only reduces the stabilization of 4 dimer relative to 3 by 5.1 kcal/mol.

Thus, the computational results on complexes 3 and 4 are supported by the experimental data. This is especially true for the magnetic data, which shows singlet ground states for these uranium(IV) complexes. While the ligands in both 3 and 4 are in fact reduced, the ligand electrons are all paired, leaving the uranium 5f orbitals as the only sites for unpaired spin density within the series of 2−4. Additionally, while the electrons are primarily restricted to the ligand, they are delocalized throughout the pyridine(diimine) plane.

Redox Reactivity. With the electronic structures of the series of 1−4 established, further demonstration of the stepwise redox chemistry was sought through reactivity studies, as analysis by electrochemical methods was not possible due to side reactions with electrolytes required for the experiments. Our previous studies for 2−4 showed that electrons stored in the ligands could undergo multi-electron oxidation in the presence of organoazides, yielding uranium imido products with neutral $^{Mes}PDI^{Me}$ ligands. While multi-electron chemistry is attractive for many chemical processes, in this case, we sought to examine single preparative electron oxidation events to demonstrate the reverse of the single electron reductions. To determine if such oxidative events were possible for 1−4, each compound was treated with molecular iodine (Scheme 1). Reactions were assayed by ^{1}H NMR spectroscopy by comparison to an authentic sample of the reaction products. Addition of 1 equiv of I_2 to dimeric 4 resulted in the quantitative formation of 3. Analogously, adding 1 equiv of I_2 to dimeric 3 produced 2 equiv of monomeric 2. One-half equivalent of I_2 effectively oxidized 2 to compound 1 as well. Using an excess of elemental iodine was successful for complete oxidation of all complexes to form 1. Oxidation reactions were also successfully performed using CuI as the oxidant. Interestingly, the oxidation of the dimeric complex 4 by 0.5 equiv of I_2, or 1 equiv of CuI, did not lead to the formation of the mixed $(^{Mes}PDI^{Me})UI$-$(^{Mes}PDI^{Me})U(THF)$ dimer but instead resulted in 0.5 molar equiv of both 3 and 4. Similarly, single electron oxidation of 3 results in the formation of an equimolar solution of 2 and 3. Thus, the stepwise ligand oxidation chemistry with iodine shown here supports the earlier claim of sequential ligand-based reduction steps in the presence of potassium graphite. Dimeric complexes 3 and 4 can serve as potent reductants toward monomeric 1 and 2 by utilizing their stored reducing equivalents. For example, dimeric 4 effectively reduces 2 to form complex 3 in quantitative yield by comproportionation. Analogous reactivity is seen in mixing 3 and 1, which generates 2.

DOI: 10.1021/ja511867a
J. Am. Chem. Soc. 2015, 137, 4690−4700

CONCLUDING REMARKS

In summary, we have described a unique series of highly reduced uranium compounds that are stabilized by the ability of the redox-active pyridine(diimine) ligand to store electron equivalents. Using spectroscopic, magnetic, and computational techniques, we have provided compelling evidence for the electronic structures of **1**−**4**. Electronic absorption spectroscopic measurements are consistent with uranium(IV) centers in each case and assignment that is corroborated by magnetometry experiments. For compound **1**, low-temperature data support the presence of a ligand radical, showing the uranium is oxidized to U(IV) and the ^{Mes}PDI^{Me} ligand is reduced upon complex formation. For compounds **2**−**4**, the magnetic data are consistent with singlet ground states for each, demonstrating uranium(IV) species. In the case of X-ray absorption spectroscopy, compound **1** seems to have a rising edge values in between U(III) and U(IV), whereas **2**−**4** match uranium(IV) standards very well. Computational experiments model the metrical parameters for **1**−**4** effectively and provide insight into the electronics of the series. In addition to supporting the spectroscopic and magnetic data, these studies establish that for **3** and **4**, there is a large driving force leading to the observed dimeric species, as evidenced by the magnitude of the calculated interaction energies. Additionally, this explains the favorable formation of the ^{Mes}PDI^{Me} ligands with formally 3− and 4− charges, the latter of which has not previously been observed.

The studies of **1**−**4** presented herein highlight the role of the redox-active ligand in stabilizing these electron-rich uranium species. Population of the low-lying π^* orbitals of ^{Mes}PDI^{Me} allows isolation of complexes that would otherwise be unstable. For instance, while compound **3** is described as a uranium(IV) species based on ligand reduction, it could *formally* be considered a monovalent uranium equivalent. This is also the case for **4**, which could be *formally* described as a source of zerovalent uranium, but spectroscopically has an oxidized uranium(IV) center. In this regard, these ligands stabilize electron-rich uranium centers in much the same way as has been observed for transition metals.[72−74] Like the metals of the d-block, our studies show that whether electrons are ligand- or metal-based, it is clear that the electrons are highly delocalized.[72]

Interestingly, there are also several important lessons to be learned in the chemistry of these redox-flexible ligands for uranium specifically. First, while uranium is not typically known for its ability to backbond effectively relative to transition metals, in the presence of few ligands besides a π-accepting ^{Mes}PDI^{Me}, backdonation can occur readily. Second, there is clearly a large driving force for the formation of uranium−arene interactions. While this has been known in the literature for some time via the synthesis of uranium−η^6−arene complexes, our theoretical results provide insight into their interaction through the calculated interaction energies gained during the dimerization reaction. Formation of the dimers featuring the actinide−arene bonds is a significant finding as compared to transition-metal chemistry with this class of ligands. With transition-metal cations, monomeric bis(pyridine(diimine)) metal complexes are formed and those compounds have limited reactivity.[32] Third, our reactivity studies presented both here and elsewhere[27,29,31] show that electrons stored in the ligand, in concert with those at uranium, are easily accessible and potent reductants for activating small molecules. Based on the synthesis of the unprecedented uranium(VI) tris(imido), (^{Mes}PDI^{Me})U(NMes)$_3$ from electron-rich **4**, future studies will be aimed toward examining the reactivity of this unique series toward small molecule activation and catalysis.

ASSOCIATED CONTENT

Supporting Information

Synthetic procedures and computational details, figures, and results. This material is available free of charge via the Internet at http://pubs.acs.org

AUTHOR INFORMATION

Corresponding Author

*sbart@purdue.edu

Notes

The authors declare no competing financial interest.

ACKNOWLEDGMENTS

The authors acknowledge support from the Division of Chemical Sciences, Geosciences, and Biosciences, Office of Basic Energy Sciences of the U.S. Department of Energy through grant DE-AC0212ER16328 (SCB), USDOE/DESC002183 (L.G. and S.O.O.), and DE-SC0006518 (E.J.S.). L.G. and S.O.O. used resources of the National Energy Research Scientific Computing Center, a DOE Office of Science User Facility supported by the Office of Science of the U.S. Department of Energy under contract no. DE-AC02-05CH11231. The XANES (S.A.K. and G.L.W.) measurements were supported under the Heavy Element Chemistry Program at LANL by the Division of Chemical Sciences, Geosciences, and Biosciences, Office of Basic Energy Sciences. Los Alamos National Laboratory is operated by Los Alamos National Security, LLC, for the National Nuclear Security Administration of U.S. Department of Energy (contract DE-AC52-06NA25396). The XANES data were obtained at the Stanford Synchrotron Radiation Lightsource (SSRL), a Directorate of SLAC National Accelerator Laboratory and an Office of Science User Facility operated for the U.S. Department of Energy Office of Science by Stanford University. The SSRL Structural Molecular Biology Program is supported by the DOE Office of Biological and Environmental Research and by the National Institutes of Health, National Institute of General Medical Sciences (including P41GM103393). The contents of this publication are solely the responsibility of the authors and do not necessarily represent the official views of NIGMS, NCRR, or NIH.

REFERENCES

(1) Lyaskovskyy, V.; de Bruin, B. *ACS Catal.* **2012**, *2*, 270.
(2) Luca, O. R.; Crabtree, R. H. *Chem. Soc. Rev.* **2013**, *42*, 1440.
(3) Kaim, W. *Eur. J. Inorg. Chem.* **2012**, *2012*, 343.
(4) Chirik, P. J. *Inorg. Chem.* **2011**, *50*, 9737.
(5) Eisenberg, R.; Gray, H. B. *Inorg. Chem.* **2012**, *50*, 9741.
(6) Chirik, P. J.; Wieghardt, K. *Science* **2010**, *327*, 794.
(7) Bejger, C.; Tian, Y.-H.; Barker, B. J.; Boland, K. S.; Scott, B. L.; Batista, E. R.; Kozimor, S. A.; Sessler, J. L. *Dalton Trans.* **2013**, *42*, 6716.
(8) Jørgensen, C. K. *Coord. Chem. Rev.* **1966**, *1*, 164.
(9) Britovsek, G. J. P.; Bruce, M.; Gibson, V. C.; Kimberley, B. S.; Maddox, P. J.; Mastroianni, S.; McTavish, S. J.; Redshaw, C.; Solan, G. A.; Stroemberg, S.; White, A. J. P.; Williams, D. J. *J. Am. Chem. Soc.* **1999**, *121*, 8728.
(10) Small, B. L.; Brookhart, M.; Bennett, A. M. A. *J. Am. Chem. Soc.* **1998**, *120*, 4049.

DOI: 10.1021/ja511867a
J. Am. Chem. Soc. 2015, 137, 4690−4700

(11) Trovitch, R. J.; Lobkovsky, E.; Bill, E.; Chirik, P. J. *Organometallics* **2008**, *27*, 1470.
(12) Hopmann, K. H. *Organometallics* **2013**, *32*, 6388.
(13) Monfette, S.; Turner, Z. R.; Semproni, S. P.; Chirik, P. J. *J. Am. Chem. Soc.* **2012**, *134*, 4561.
(14) Russell, S. K.; Darmon, J. M.; Lobkovsky, E.; Chirik, P. J. *Inorg. Chem.* **2010**, *49*, 2782.
(15) Bart, S. C.; Lobkovsky, E.; Chirik, P. J. *J. Am. Chem. Soc.* **2004**, *126*, 13794.
(16) Pal, R.; Groy, T. L.; Bowman, A. C.; Trovitch, R. J. *Inorg. Chem.* **2014**, *53*, 9357.
(17) Tondreau, A. M.; Lobkovsky, E.; Chirik, P. J. *Org. Lett.* **2008**, *10*, 2789.
(18) Tondreau, A. M.; Darmon, J. M.; Wile, B. M.; Floyd, S. K.; Lobkovsky, E.; Chirik, P. J. *Organometallics* **2009**, *28*, 3928.
(19) Obligacion, J. V.; Chirik, P. J. *J. Am. Chem. Soc.* **2013**, *135*, 19107.
(20) Obligacion, J. V.; Chirik, P. J. *Org. Lett.* **2013**, *15*, 2680.
(21) Hoyt, J. M.; Sylvester, K. T.; Semproni, S. P.; Chirik, P. J. *J. Am. Chem. Soc.* **2013**, *135*, 4862.
(22) Takeuchi, D.; Matsuura, R.; Park, S.; Osakada, K. *J. Am. Chem. Soc.* **2007**, *129*, 7002.
(23) Sylvester, K. T.; Chirik, P. J. *J. Am. Chem. Soc.* **2009**, *131*, 8772.
(24) Biernesser, A. B.; Li, B.; Byers, J. A. *J. Am. Chem. Soc.* **2013**, *135*, 16553.
(25) Shejwalkar, P.; Rath, N. P.; Bauer, E. B. *Synthesis* **2014**, *46*, 57.
(26) Myers, T. W.; Berben, L. A. *Chem. Sci.* **2014**, *5*, 2771.
(27) Kiernicki, J. J.; Newell, B. S.; Matson, E. M.; Anderson, N. H.; Fanwick, P. E.; Shores, M. P.; Bart, S. C. *Inorg. Chem.* **2014**, *53*, 3730.
(28) Cladis, D. P.; Kiernicki, J. J.; Fanwick, P. E.; Bart, S. C. *Chem. Commun.* **2013**, *49*, 4169.
(29) Anderson, N. H.; Odoh, S. O.; Yao, Y.; Williams, U. J.; Schaefer, B. A.; Kiernicki, J. J.; Lewis, A. J.; Goshert, M. D.; Fanwick, P. E.; Schelter, E. J.; Walensky, J. R.; Gagliardi, L.; Bart, S. C. *Nat. Chem.* **2014**, *6*, 919.
(30) Knijnenburg, Q.; Gambarotta, S.; Budzelaar, P. H. M. *Dalton Trans.* **2006**, 5442.
(31) Kiernicki, J. J.; Fanwick, P. E.; Bart, S. C. *Chem. Commun.* **2014**, *50*, 8189.
(32) Wile, B. M.; Trovitch, R. J.; Bart, S. C.; Tondreau, A. M.; Lobkovsky, E.; Milsmann, C.; Bill, E.; Wieghardt, K.; Chirik, P. J. *Inorg. Chem.* **2009**, *48*, 4190.
(33) Evans, W. J.; Kozimor, S. A. *Coord. Chem. Rev.* **2006**, *250*, 911.
(34) Korobkov, I.; Gambarotta, S. *Prog. Inorg. Chem.* **2005**, *54*, 321.
(35) Fox, A. R.; Bart, S. C.; Meyer, K.; Cummins, C. C. *Nature* **2008**, *455*, 341.
(36) Duhovic, S.; Oria, J. V.; Odoh, S. O.; Schreckenbach, G.; Batista, E. R.; Diaconescu, P. L. *Organometallics* **2013**, *32*, 6012.
(37) Bart, S. C.; Heinemann, F. W.; Anthon, C.; Hauser, C.; Meyer, K. *Inorg. Chem.* **2009**, *48*, 9419.
(38) Castro-Rodriguez, I.; Olsen, K.; Gantzel, P.; Meyer, K. *J. Am. Chem. Soc.* **2003**, *125*, 4565.
(39) Morris, D. E.; Re, R. E. D.; Jantunen, K. C.; Castro-Rodriguez, I.; Kiplinger, J. L. *Organometallics* **2004**, *23*, 5142.
(40) Bart, S. C.; Anthon, C.; Heinemann, F. W.; Bill, E.; Edelstein, N. M.; Meyer, K. *J. Am. Chem. Soc.* **2008**, *130*, 12536.
(41) Lam, O. P.; Feng, P. L.; Heinemann, F. W.; O'Connor, J. M.; Meyer, K. *J. Am. Chem. Soc.* **2008**, *130*, 2806.
(42) Lam, O. P.; Anthon, C.; Heinemann, F. W.; O'Connor, J. M.; Meyer, K. *J. Am. Chem. Soc.* **2008**, *130*, 6567.
(43) Castro-Rodriguez, I.; Nakai, H.; Zakharov, L. N.; Rheingold, A. L.; Meyer, K. *Science* **2004**, *305*, 1757.
(44) Schelter, E. J.; Morris, D. E.; Scott, B. L.; Thompson, J. D.; Kiplinger, J. L. *Inorg. Chem.* **2007**, *46*, 5528.
(45) Kindra, D. R.; Evans, W. J. *Chem. Rev.* **2014**, *114*, 8865.
(46) Kozimor Stosh, A.; Bartlett, B. M.; Rinehart, J. D.; Long, J. R. *J. Am. Chem. Soc.* **2007**, *129*, 10672.
(47) Salmon, L.; Thuery, P.; Riviere, E.; Miyamoto, S.; Yamato, T.; Ephritikhine, M. *New J. Chem.* **2006**, *30*, 1220.
(48) Cooper, O. J.; Mills, D. P.; McMaster, J.; Moro, F.; Davies, E. S.; Lewis, W.; Blake, A. J.; Liddle, S. T. *Angew. Chem., Int. Ed.* **2011**, *50*, 2383.
(49) Schelter, E. J.; Veauthier, J. M.; Graves, C. R.; John, K. D.; Scott, B. L.; Thompson, J. D.; Pool-Davis-Tournear, J. A.; Morris, D. E.; Kiplinger, J. L. *Chem.—Eur. J.* **2008**, *14*, 7782.
(50) Schelter, E. J.; Wu, R.; Scott, B. L.; Thompson, J. D.; Cantat, T.; John, K. D.; Batista, E. R.; Morris, D. E.; Kiplinger, J. L. *Inorg. Chem.* **2010**, *49*, 924.
(51) Jilek, R. E.; Spencer, L. P.; Kuiper, D. L.; Scott, B. L.; Williams, U. J.; Kikkawa, J. M.; Schelter, E. J.; Boncella, J. M. *Inorg. Chem.* **2011**, *50*, 4235.
(52) Vlaisavljevich, B.; Diaconescu, P. L.; Lukens, W. L., Jr.; Gagliardi, L.; Cummins, C. C. *Organometallics* **2013**, *32*, 1341.
(53) Kosog, B.; La, P. H. S.; Denecke, M. A.; Heinemann, F. W.; Meyer, K. *Inorg. Chem.* **2012**, *51*, 7940.
(54) Brendebach, B.; Banik, N. L.; Marquardt Christian, M.; Rothe, J.; Denecke, M.; Geckeis, H. *Radiochim. Acta* **2009**, *97*, 701.
(55) Chiang, M.-H.; Williams, C. W.; Soderholm, L.; Antonio, M. R. *Eur. J. Inorg. Chem.* **2003**, *2003*, 2663.
(56) Kraft, S. J.; Williams, U. J.; Daly, S. R.; Schelter, E. J.; Kozimor, S. A.; Boland, K. S.; Kikkawa, J. M.; Forrest, W. P.; Christensen, C. N.; Schwarz, D. E.; Fanwick, P. E.; Clark, D. L.; Conradson, S. D.; Bart, S. C. *Inorg. Chem.* **2011**, *50*, 9838.
(57) Lukens, W. W., Jr.; Allen, P. G.; Bucher, J. J.; Edelstein, N. M.; Hudson, E. A.; Shuh, D. K.; Reich, T.; Andersen, R. A. *Organometallics* **1999**, *18*, 1253.
(58) Andersen, R. A. *Inorg. Chem.* **1979**, *18*, 1507.
(59) Fagan, P. J.; Manriquez, J. M.; Marks, T. J.; Day, C. S.; Vollmer, S. H.; Day, V. W. *Organometallics* **1982**, *1*, 170.
(60) Evans, W. J.; Nyce, G. W.; Forrestal, K. J.; Ziller, J. W. *Organometallics* **2002**, *21*, 1050.
(61) Clark, D. L.; Sattelberger, A. P.; Bott, S. G.; Vrtis, R. N. *Inorg. Chem.* **1989**, *28*, 1771.
(62) Avens, L. R.; Bott, S. G.; Clark, D. L.; Sattelberger, A. P.; Watkin, J. G.; Zwick, B. D. *Inorg. Chem.* **1994**, *33*, 2248.
(63) Minasian, S. G.; Boland, K. S.; Feller, R. K.; Gaunt, A. J.; Kozimor, S. A.; May, I.; Reilly, S. D.; Scott, B. L.; Shuh, D. K. *Inorg. Chem.* **2012**, *51*, 5728.
(64) Spencer, L. P.; Yang, P.; Minasian, S. G.; Jilek, R. E.; Batista, E. R.; Boland, K. S.; Boncella, J. M.; Conradson, S. D.; Clark, D. L.; Hayton, T. W.; Kozimor, S. A.; Martin, R. L.; MacInnes, M. M.; Olson, A. C.; Scott, B. L.; Shuh, D. K.; Wilkerson, M. P. *J. Am. Chem. Soc.* **2013**, *135*, 2279.
(65) Kraft, S. J.; Walensky, J.; Fanwick, P. E.; Hall, M. B.; Bart, S. C. *Inorg. Chem.* **2010**, *49*, 7620.
(66) Matson, E. M.; Goshert, M. D.; Kiernicki, J. J.; Newell, B. S.; Fanwick, P. E.; Shores, M. P.; Walensky, J. R.; Bart, S. C. *Chem.—Eur. J.* **2013**, *19*, 16176.
(67) Nalewajski, R. F.; Mrozek, J.; Mazur, G. *Can. J. Chem.* **1996**, *74*, 1121.
(68) Enright, D.; Gambarotta, S.; Yap, G. P. A.; Budzelaar, P. H. M. *Angew. Chem., Int. Ed.* **2002**, *41*, 3873.
(69) Tondreau, A. M.; Stieber, S. C. E.; Milsmann, C.; Lobkovsky, E.; Weyhermüller, T.; Semproni, S. P.; Chirik, P. J. *Inorg. Chem.* **2013**, *52*, 635.
(70) Grimme, S.; Antony, J.; Ehrlich, S.; Krieg, H. *J. Chem. Phys.* **2010**, *132*, 154104.
(71) Burke, K. *J. Chem. Phys.* **2012**, *136*, 150901.
(72) Bart, S. C.; Chlopek, K.; Bill, E.; Bouwkamp, M. W.; Lobkovsky, E.; Neese, F.; Wieghardt, K.; Chirik, P. J. *J. Am. Chem. Soc.* **2006**, *128*, 13901.
(73) Bowman, A. C.; Milsmann, C.; Hojilla Atienza, C. C.; Lobkovsky, E.; Wieghardt, K.; Chirik, P. J. *J. Am. Chem. Soc.* **2010**, *132*, 1676.
(74) Stieber, S. C. E.; Milsmann, C.; Hoyt, J. M.; Turner, Z. R.; Finkelstein, K. D.; Wieghardt, K.; DeBeer, S.; Chirik, P. J. *Inorg. Chem.* **2012**, *51*, 3770.

DOI: 10.1021/ja511867a
J. Am. Chem. Soc. 2015, 137, 4690−4700